eprints@whiterose.ac.uk
https://eprints.whiterose.ac.uk/

Gradient elasticity: a transformative stress analysis tool to design notched components against uniaxial/multiaxial high-cycle fatigue

Cristian Bagni, Harm Askes, Luca Susmel

Department of Civil and Structural Engineering, The University of Sheffield, Mappin Street, Sheffield S1 3JD, United Kingdom

Corresponding Author: Prof. **Luca Susmel**
Department of Civil and Structural Engineering
The University of Sheffield, Mappin Street, Sheffield, S1 3JD, UK
Telephone: +44 (0) 114 222 5073
Fax: +44 (0) 114 222 5700
e-mail: l.susmel@sheffield.ac.uk

Abstract

This paper investigates the accuracy of gradient elasticity in estimating high-cycle fatigue strength of notched components subjected to both uniaxial and multiaxial fatigue loading. A novel design methodology is formulated by combining Ru and Aifantis' gradient elasticity with the Theory of Critical Distances and the Modified Wöhler Curve Method. The key-feature of this innovative design methodology is that, via the Theory of Critical Distances, gradient elasticity's length scale parameter is directly estimated from conventional material fatigue properties (i.e., the plain fatigue limit and the threshold value of the stress intensity factor). From a stress analysis point of view, the proposed approach directly post-processes the gradient-enriched stress states determined, at the hot-spots, on the surface of the component under investigation (and independently of the sharpness of the stress concentrator being assessed). The accuracy and reliability of this design method was checked by using a large number of experimental results taken from the literature and generated by testing notched metallic samples under uniaxial as well as under multiaxial fatigue loading. This comprehensive validation exercise demonstrates that the systematic usage of this transformative design approach leads to the same level of accuracy as the one which is obtained by applying the classic Theory of Critical Distances. This result is certainly remarkable since the proposed approach is not only very efficient from a computational point of view, but it also allows high-cycle fatigue damage to be assessed by directly post-processing gradient-enriched stress states determined on the surface of the component being assessed.

Keywords: Gradient Elasticity; Theory of Critical Distances; Fatigue; Notch

Nomenclature

r, θ = local polar coordinates
R = load ratio
K_f = fatigue strength reduction factor
ΔK_{th} = range of the threshold value of the stress intensity factor
r_n = root radius
n = outward normal to the boundary

ρ_{eff} = critical plane stress ratio

ρ_{eff}^g = gradient-enriched critical plane stress ratio at the hot-spot

ρ_{lim} = limit value of the critical plane stress ratio

ρ_{lim}^g = limit value of the gradient-enriched critical plane stress ratio at the hot-spot
m = mean stress sensitivity index
N_f = number of cycles to failure
N_o = reference number of cycles to failure
K_t = stress concentration factor under uniaxial loading
K_{tt} = stress concentration factor under torsion
k_τ = negative inverse slope of the modified Wöhler curve
α, β, a, b = material constants in the MWCM approach
L = critical distance
ℓ = gradient elasticity length scale parameter
C_{ijkl} = elastic tensor
b_i = body forces
u_k = displacements

u_k^c = classical (or local) displacements

u_k^g = gradient-enriched (or non-local) displacements

ε_{ij} = infinitesimal strain tensor
σ_{ij} = Cauchy's stress tensor

σ_{ij}^g = gradient-enriched (or non-local) stress tensor

$\Delta\sigma_{eff}$ = range of the effective stress
$\Delta\sigma_y$ = range of the linear-elastic normal stress
$\Delta\sigma_y^g$ = range of the gradient-enriched normal stress at the notch tip

$\Delta\sigma_o$ = range of the plain fatigue limit

$\Delta\sigma_o^g$ = gradient-enriched range of the plain fatigue limit at the surface of the specimen

$\sigma_{n,m}$ = mean value of the stress normal to the critical plane

$\sigma_{n,m}^g$ = gradient-enriched mean value of the stress normal to the critical plane at the hot-spot

$\sigma_{n,a}$ = amplitude of the stress normal to the critical plane

$\sigma_{n,a}^g$ = gradient-enriched amplitude of the stress normal to the critical plane at the hot-spot

σ_o = fully-reversed uniaxial fatigue limit at N_o cycles to failure

σ_o^g = gradient-enriched uniaxial fatigue limit at the surface of the specimen

τ_a = shear stress amplitude on the critical plane

τ_a^g = gradient-enriched shear stress amplitude on the critical plane at the hot-spot

τ_{Ref} = reference shear stress amplitude estimated at N_o cycles

τ_o = fully-reversed torsional fatigue limit at N_o cycles to failure

τ_o^g = gradient-enriched torsional fatigue limit at the surface of the specimen

τ_{eq} = equivalent shear stress

τ_{eq}^g = gradient-enriched equivalent shear stress at the hot-spot

t = generic time instant

F_o = amplitude of the external uniaxial force in the fatigue limit condition

M_o = amplitude of the external bending moment in the fatigue limit condition

T_o = amplitude of the external torsional moment in the fatigue limit condition

$E_\sigma[\%]$ = fatigue strength error index for Mode I fatigue loading

$E_\tau[\%]$ = fatigue strength error index for multiaxial fatigue loading

INTRODUCTION

The complex geometries of real mechanical components often result in local stress concentration phenomena that affect the overall fatigue strength of the components themselves. According to the classic method due to Neuber [1] and Peterson [2], the detrimental effect of stress raisers can be taken into account by correcting the plain material SN curve via the so-called fatigue strength reduction factor, K_f. Owing to the fact that the stress analysis has to be performed in terms of nominal net stresses, the in-field usage of this approach requires the definition of suitable nominal net cross-sectional areas. Unfortunately, in the presence of complex three-dimensional geometries this is not always straightforward, leading to possible design ambiguities and errors.

As far as high-cycle fatigue strength is concerned, the extent of fatigue damage can somehow be quantified also in terms of linear-elastic notch tip stresses [3]. The advantage of this simplified approach is that linear-elastic notch root stresses can easily be determined via conventional linear-elastic finite element (FE) models. However, even if this FE based methodology is very straightforward, the resulting level of conservatism is seen to increase as the sharpness of the geometrical feature being assessed increases [3]. Therefore, under relatively large values of the stress concentration factors, this leads to components and structures which are heavier and bigger than necessary, with a consequent inefficient usage of materials and energy. Further, this simplified approach cannot be used to design against

fatigue cracks and sharp notches, since the resulting linear-elastic local stress fields become singular when crack/notch tip radii are taken equal to zero.

Examination of the state of the art shows that in recent years different theories have been devised to specifically perform the high-cycle fatigue assessment of notched components without missing the undoubted advantages of linear-elastic FE solutions. In this context, the so-called Theory of Critical Distances (TCD) [3] has proven to be a reliable design tool capable of accurately estimating high-cycle fatigue strength of components containing stress risers of all kinds. Taking as a starting point Neuber and Peterson's ideas [1, 2], the TCD postulates that the extent of fatigue damage can be quantified via an effective stress whose magnitude depends not only on the local linear-elastic stress fields in the vicinity of the assumed crack initiation locations, but also on a specific material characteristic length. In the TCD framework, such a critical distance is treated as a material property whose value changes as the load ratio varies (mean stress effect in fatigue). However, despite its undoubted accuracy and advantages, using the TCD to post-process linear-elastic stress fields determined from FE models is not only cumbersome, but also demanding from a computational viewpoint, a very refined mesh being required to accurately determine the local stress fields in the presence of sharp notches and cracks.

To overcome these problems, the TCD can efficiently be applied numerically by reinterpreting it in terms of gradient elasticity [4]. Gradient elasticity assumes that the relevant stress fields ahead of crack/notch tips have to be calculated by directly incorporating a length scale parameter into the adopted constitutive law, such a characteristic length being representative of the underlying material microstructure.

Recently, the analogies between the TCD and gradient elasticity were investigated in detail and an explicit relationship between the length scale parameters used by these two approaches was established (see Refs [5-7]). In this context, Tovo and Livieri have recently proven that the so-called implicit gradient approach (which represents a particular way of

using gradient elasticity) is successful in estimating high-cycle fatigue strength of welded joints [8, 9].

In this complex scenario, the aim of the present paper is to formulate an alternative fatigue design approach which combines the TCD's accuracy in estimating high-cycle notch fatigue strength with the computational efficiency of gradient elasticity in determining non-local stress fields in the vicinity of finite radius stress raisers.

GRADIENT ELASTICITY

Gradient elasticity represents a family of theories which allows the influence of the underlying material microstructure to be taken into account directly. This is possible by enriching the constitutive relations through high-order gradients of the relevant state variables together with intrinsic length scale parameters. One of the most important advantages of gradient elasticity is its ability to remove singularities from the linear-elastic stress fields in the vicinity of cracks and sharp notches. Further, as far as finite radius stress concentrators are concerned, the use of gradient elasticity leads to linear-elastic stress fields having a magnitude lower than the corresponding one determined according to classic continuum mechanics.

In this paper, the theory developed by Aifantis and co-workers in the early 1990s [4, 10, 11] and recently implemented in a unified finite element framework [12, 13] is considered. This approach consists in enriching the constitutive relations with the Laplacian of the strains as follows:

$$\sigma_{ij} = C_{ijkl}\left(\varepsilon_{kl} - \ell^2 \varepsilon_{kl,mm}\right) \tag{1}$$

where σ_{ij} is the Cauchy stress tensor, ε_{ij} is the infinitesimal strain tensor, C_{ijkl} is the elastic constitutive tensor and ℓ is an intrinsic material length scale parameter. Eq. (1) leads to the following equilibrium equations:

$$C_{ijkl}\left(u_{k,jl} - \ell^2\varepsilon_{k,jlmm}\right) + b_i = 0 \tag{2}$$

where u_k are the displacements and b_i the body forces.

Eq. (2) represents a system of fourth-order partial differential equations which require continuity of displacements and their first derivatives, with significant complications in the finite element implementation. However, in the 1990s Ru and Aifantis [4] proposed a theorem, consisting in a factorisation of the derivatives, which allows the solution of Eq. (2) to be calculated as two uncoupled systems of second-order partial differential equations. This results in a straightforward and effective C^0 finite element implementation [12, 13].

The first step of the aforementioned theorem consists in the solution of the standard equations of classical elasticity:

$$C_{ijkl}u_{k,jl}^c + b_i = 0 \tag{3}$$

where u_k^c are the classical (or local) displacements.

Using then the calculated local displacements u_k^c as source terms, it is possible to solve the following second system of partial differential equations:

$$u_k^g - \ell^2 u_{k,mm}^g = u_k^c \tag{4}$$

where u_k^g are the gradient-enriched (or non-local) displacements.

In the finite element methodology discussed in Refs [12, 13] and used for the numerical simulations in the present investigation, the second step was considered in terms of stresses as follows:

$$\sigma_{ij}^{g} - \ell^{2}\sigma_{ij,mm}^{g} = C_{ijkl}u_{k,l}^{c} \tag{5}$$

which is obtained from Eq. (4) after differentiation and pre-multiplication with C_{ijkl}. This stress-based formulation has several advantages over the displacement-based approach as explained in detail in Refs [14-16].

As to the in-field usage of gradient elasticity, while for the first step the boundary conditions are clearly defined and they consist in the usual choice between essential or natural boundary conditions, the definition of the best boundary conditions for the second step is still subject to some debate. However, the application of homogeneous natural boundary conditions throughout the boundary is widely accepted as the best option to be used.

THEORY OF CRITICAL DISTANCES

As stated by Taylor [3], the TCD represents a family of methods that are all characterised by two main common features: (i) the relevant stress fields are determined by adopting a simple linear-elastic constitutive law to model the mechanical behaviour of the material being assessed; (ii) the extent of damage is assessed via an effective stress whose value depends not only on the entire linear-elastic stress fields acting on the material in the vicinity of the crack initiation locations, but also on a material characteristic length.

Independently of the strategy which is followed to formalise the TCD, this approach assumes that in the high-cycle fatigue regime the threshold condition for the non-propagation of a crack can directly be expressed as follows [17]:

$$\Delta\sigma_{eff} \leq \Delta\sigma_{o} \tag{6}$$

where $\Delta\sigma_{eff}$ is the range of the effective stress (which is a function also of a material critical distance), whereas $\Delta\sigma_o$ is the plain fatigue limit range (determined under the load ratio, $R=\sigma_{min}/\sigma_{max}$, of interest).

Examination of the state of the art [3] shows that the TCD has been formulated in different ways which include the Point, Line, and Area Method. The common feature of these different formalisations of the TCD is that the required critical distance can directly be determined from the plain fatigue limit range, $\Delta\sigma_o$, and the threshold value of the stress intensity factor range, ΔK_{th}, as follows [17-19]:

$$L = \frac{1}{\pi}\left(\frac{\Delta K_{th}}{\Delta\sigma_o}\right)^2 \qquad (7)$$

It is important to point out here that critical distance L has to be estimated by using values for $\Delta\sigma_o$ and ΔK_{th} determined under the same load ratio, R, as the one characterising the load history applied to the component being assessed.

Turning back to the different formalisations of the TCD, the Point Method (PM) –that was first proposed by Peterson [2] - postulates that the range of the effective stress has to be calculated at a distance from the stress concentrator being assessed equal to L/2, i.e. [17] (see also Figure 1b):

$$\Delta\sigma_{eff} = \Delta\sigma_y\left(\theta = 0, r = \frac{L}{2}\right) \qquad (8)$$

According to Neuber's idea [1], the Line Method (LM) instead calculates $\Delta\sigma_{eff}$ by averaging $\Delta\sigma_y$ over a line of length 2L, i.e. [17] (see also Figure 1c):

$$\Delta\sigma_{eff} = \frac{1}{2L}\int_0^{2L}\Delta\sigma_y\left(\theta=0,r\right)dr \tag{9}$$

Finally, as suggested by Sheppard [20], the Area Method (AM) calculates $\Delta\sigma_{eff}$ by averaging $\Delta\sigma_y$ over a semi-circular area of radius L and centred at the notch tip. The range of the effective stress $\Delta\sigma_{eff}$ is then determined as [3, 17] (see also Figure 1d):

$$\Delta\sigma_{eff} = \frac{4}{\pi L^2}\int_0^{\pi/2}\int_0^L\Delta\sigma_y\left(\theta,r\right)r\cdot dr\cdot d\theta \tag{10}$$

where r and θ are the local polar coordinates in a reference system centred at the notch tip (see Figure 1a).

EXTENDING THE USE OF THE PM TO MULTIAXIAL FATIGUE SITUATIONS

The TCD as reviewed in the previous section can be applied solely to notches subjected to in-service Mode I fatigue loading. In order to extend its use to those situations involving complex multiaxial load histories, this approach has to be applied along with an appropriate multiaxial fatigue damage model [21, 22]. By performing a systematic validation exercise based on a large number of experimental results [21, 23, 24], it has been proven that the highest level of accuracy is obtained by applying the PM along with the so-called Modified Wöhler Curve Method (MWCM) [21, 25, 26].

The MWCM is a bi-parametrical critical plane approach, the critical plane being that material plane experiencing the maximum shear stress amplitude, τ_a. The MWCM quantifies the extent of fatigue damage not only via τ_a, but also via the mean value, $\sigma_{n,m}$, and the amplitude, $\sigma_{n,a}$, of the stress perpendicular to the critical plane. The damaging effect of these three stress components is assessed through the critical plane stress ratio which is defined as [26]:

$$\rho_{eff} = \frac{m \cdot \sigma_{n,m} + \sigma_{n,a}}{\tau_a} \tag{11}$$

In definition (11) m is the mean stress sensitivity index [26], i.e., a material property whose value (ranging in the interval 0-1) has to be determined by running appropriate experiments [21, 27]. The most remarkable feature of ratio ρ_{eff} is that it is sensitive not only to the presence of non-zero mean stresses, but also to the degree of multiaxiality of the load history being assessed [21].

The way the MWCM assesses fatigue strength under multiaxial fatigue loading is shown in the modified Wöhler diagram of Figure 2a. This log-log chart plots τ_a against the number of cycles to failure, N_f. If this schematisation is used to describe the multiaxial fatigue behaviour of metallic materials, much experimental evidence [21, 25, 26] suggests that different fatigue curves are obtained as ratio ρ_{eff} varies (Fig. 2a). The position and the negative inverse slope of any Modified Wöhler curve can then be defined via the following relationships [21, 25, 26]:

$$k_\tau\left(\rho_{eff}\right) = \alpha \cdot \rho_{eff} + \beta \tag{12}$$

$$\tau_{Ref}\left(\rho_{eff}\right) = a \cdot \rho_{eff} + b \tag{13}$$

In Eqs (12) and (13) $k_\tau(\rho_{eff})$ is the negative inverse slope, $\tau_{Ref}(\rho_{eff})$ is the reference shear stress amplitude (i.e., the endurance limit) estimated at N_o cycles to failure (see Figure 2a), and α, β, a and b are material constants to be determined by running appropriate experiments [21]. By observing that ρ_{eff} is equal to unity under fully-reversed uniaxial cyclic loading and to zero under torsional cyclic loading [21, 25], Eq. (13) suggests that, according to the MWCM's *modus operandi*, fatigue damage is assumed to increase as ρ_{eff} increases. If σ_o and τ_o are

used to denote the endurance limits extrapolated at N_o cycles to failure under fully-reversed uniaxial and torsional fatigue loading, respectively, then relationship (13) can be rewritten as follows:

$$\tau_{Ref}(\rho_{eff}) = \left(\frac{\sigma_o}{2} - \tau_o \right) \cdot \rho_{eff} + \tau_o \tag{14}$$

According to the Modified Wöhler diagram of Figure 2a, the material being investigated is in the endurance limit condition as long as τ_a is lower than (or, at least, equal to) the reference shear stress estimated via Eq. (14) for the value of ratio ρ_{eff} characterising the cyclic state of stress relative to the critical plane, i.e.:

$$\tau_a \leq \tau_{Ref}(\rho_{eff}) = \left(\frac{\sigma_o}{2} - \tau_o \right) \cdot \rho_{eff} + \tau_o \Rightarrow$$

$$\Rightarrow \tau_{eq} = \tau_a - \left(\frac{\sigma_o}{2} - \tau_o \right) \cdot \rho_{eff} \leq \tau_o \tag{15}$$

where τ_{eq} can be treated as an equivalent shear stress.

The MWCM formalised according to Eq. (15) can be used as long as fatigue damage is mainly governed by the shear stress amplitude relative to the critical plane. On the contrary, under large values of ratio ρ_{eff}, the estimates obtained via criterion (15) are seen to be characterised by an excessive level of conservatism [28]. This can be ascribed to the fact that, when micro/meso cracks are fully open, an increase of the normal mean stress does not lead to a further increase of the associated fatigue damage [26, 29]. According to this reasoning, Eq. (15) is recommended to be corrected as shown in the τ_a vs. ρ_{eff} chart of Figure 2b [21, 26]. As suggested by this schematic diagram, the material being assessed is in the endurance limit

condition as long as τ_a is below the limit curve determined according to criterion (15) up to a value of ρ_{eff} equal to ρ_{lim}, where [21, 26]:

$$\rho_{lim} = \frac{\tau_o}{2\tau_o - \sigma_o} \qquad (16)$$

For $\rho_{eff} > \rho_{lim}$, the reference shear stress to be used to estimate multiaxial fatigue damage is assumed instead to be constant and invariably equal to $\tau_{Ref}(\rho_{lim})$ [21, 26] – see Figure 2b.

The MWCM can directly be applied along with the TCD (used in the form of the PM) to assess notched components subjected to multiaxial fatigue loading [21, 23, 24]. In particular, the scale and the stress gradient effect are taken into account via the TCD, whereas the MWCM assesses the degree of multiaxiality and non-proportionality of the local stress fields [21].

In order to correctly apply the MWCM along with the PM, the material fatigue properties needed to estimate m, a, b, and ρ_{lim} in Eqs (11), (13) and (16) have to be determined by using experimental fatigue results generated by testing under fully-reversed loading un-notched specimens, critical distance L being estimated according to definition (7). It is important to point out here that to use the MWCM in conjunction with the PM, material length L is recommended to be estimated by determining both $\Delta\sigma_o$ and ΔK_{th} under fully-reversed fatigue loading. This is due the fact that the detrimental effect of non-zero mean stresses is directly assessed by the MWCM itself [21].

Figure 2c shows how the MWCM is recommended to be used along with the PM to assess the high-cycle fatigue strength of notched components. In more detail, the component sketched in this figure is assumed to be subjected to a complex system of cyclic forces and cyclic moments leading to a time-variable multiaxial stress state acting on the material in the vicinity of the assumed crack initiation site (point A in Figure 2c). The focus path used to apply the TCD in the form of the PM emanates from point A and is perpendicular to the

surface (see Figure 2c). The critical point, O, at which the relevant state of stress has to be determined is positioned, along the focus path itself, at a distance from the assumed crack initiation point equal to L/2. By adopting a suitable local frame of reference, Oxyz, the linear-elastic stress state at point O is as follows (Fig. 2c):

$$[\sigma(t)] = \begin{bmatrix} \sigma_x(t) & \tau_{xy}(t) & \tau_{xz}(t) \\ \tau_{xy}(t) & \sigma_y(t) & \tau_{yz}(t) \\ \tau_{xz}(t) & \tau_{yz}(t) & \sigma_z(t) \end{bmatrix} \qquad (17)$$

where t is time. τ_a, $\sigma_{n,m}$ and $\sigma_{n,a}$ can now be calculated by directly post-processing tensor (17) [30, 31]. Subsequently, these stress components have to be used to estimate, according to definition (11), the effective value of the critical plane stress ratio, ρ_{eff}. Finally, as shown in Figure 2b, the notched component being assessed is assumed to be in the fatigue limit condition as long as τ_a is below the limit curve determined by calibrating the MWCM through the un-notched material fatigue properties (see also Figure 2c).

COMBINING GRADIENT ELASTICITY WITH THE TCD AND THE MWCM

Although it is widely accepted that length scale parameter ℓ is related to the size of the dominant source of microstructural heterogeneity [15], examination of the state of the art suggests that the scientific community has yet to agree on a commonly accepted strategy suitable for estimating ℓ to use gradient elasticity in situations of practical interest.

As to a possible way to determine length ℓ, the previous sections should make it evident that gradient elasticity and the TCD share some important features. In particular, both approaches post-process the relevant stress fields by coupling liner-elasticity with an internal length scale parameter which is assumed to be an intrinsic material property. By taking as a starting point these similarities, recently it was proven that length ℓ can directly be estimated from the TCD's critical distance L as follows [6]:

$$\ell \approx \frac{L}{2\sqrt{2}} = \frac{1}{2\sqrt{2}\pi}\left(\frac{\Delta K_{th}}{\Delta\sigma_o}\right)^2 \tag{18}$$

The above relationship was derived by considering a cracked plate subjected to Mode I loading, the stress field in the vicinity of the crack tip being post-processed by following a fairly articulated reasoning based on local mechanics [6]. According to Eq. (18), length scale parameter ℓ can directly be estimated from the material plain fatigue limit, $\Delta\sigma_o$, and the threshold value of the stress intensity factor range, ΔK_{th}. Since both $\Delta\sigma_o$ and ΔK_{th} are material properties, ℓ is in turn an intrinsic characteristic length which is different for different materials and different load ratios. As to the validity of this way of estimating ℓ, by post-processing a large number of experimental results taken from the literature, gradient elasticity was seen to be capable of accurately modelling, in the fatigue limit condition, the transition from the short- to the long-crack regime [6]. Another important aspect is that, compared to the numerical effort required to apply the conventional TCD to model cracks, the use of gradient elasticity allowed us to reduce the computational time by at least 50%.

In light of the encouraging results obtained by considering cracked materials, the next logical step in the development of this design approach is then verifying whether length ℓ estimated via Eq. (18) is suitable also for assessing high-cycle fatigue strength in the presence of finite radius stress concentrators.

The way gradient elasticity works when it is used to post-process the local stress fields according to the TCD is explained in Figure 3a, with this schematisation being valid proved that ℓ is directly derived from L through Eq. (18). As shown in Figure 3a, gradient elasticity can simply be thought of as an operator transferring the PM linear elastic stress state determined at a distance from the notch tip equal to L/2 onto the surface of the notch itself (Fig. 3a). According to this idea, high-cycle fatigue strength of notched components can then

be assessed by directly using the maximum gradient-enriched stress state determined at the apex of the geometrical feature being assessed.

To use gradient elasticity consistently, the second problem to address is the definition of appropriate reference un-notched fatigue (endurance) limits. Figures 3b, 3c and 3d show the stress distributions in a smooth cylindrical shaft loaded in cyclic tension-compression (Fig. 3b), cyclic bending (Fig. 3c) and cyclic torsion (Fig. 3d). These three bars are assumed to be made of the same metallic material, so that length scale ℓ is the same independently of the type of applied loading. In these sketches symbols F_o, M_o and T_o are used to denote the amplitudes of the external forces and moments in the fatigue (endurance) limit condition. As shown in Figures 3c and 3d, the gradient-enriched fatigue (endurance) limits at the surface of the shaft, σ_o^g and τ_o^g, are lower than the corresponding ones, σ_o and τ_o, calculated according to continuum mechanics. This is due to the fact that in the presence of stress gradients Ru and Aifantis' gradient elasticity smoothens the local stress fields via length scale parameter ℓ, irrespective of the source generating the stress gradients themselves. Solely in the absence of stress gradients – as it happens, for instance, under cyclic axial loading (Fig. 3a) - the use of gradient elasticity returns the same stress fields as those determined according to continuum mechanics. Therefore, in situations of practical interest, gradient elasticity should be used by adopting σ_o^g and τ_o^g as reference un-notched fatigue (endurance) limits [32]. However, it has to be said that, in general, under both cyclic bending and cyclic torsion the difference between conventional and gradient-enriched fatigue (endurance) limits is seen to be very little (on average, lower than about 5%). This suggests that σ_o and τ_o can still be used as reference fatigue strengths, provided that a little loss of accuracy is considered to be acceptable when performing the high-cycle fatigue assessment.

Figures 4a and 4b summarise the procedures which are suggested here as being followed to design notched components against uniaxial and multiaxial high-cycle fatigue, respectively.

For the sake of simplicity, initially attention can be focussed solely on the simpler uniaxial fatigue problem. Consider then the notch sketched in Figure 4a which is assumed to be

subjected to Mode I cyclic loading. According to the procedure summarised in Figure 4a, the range of the gradient-enriched stress at the notch tip, $\Delta\sigma_y^g$, has to be determined by solving a linear-elastic gradient elasticity FE model - with ℓ being estimated from L via Eq. (18). The component being assessed is assumed to be at its fatigue (endurance) limit as long as the following condition is assured:

$$\Delta\sigma_y^g \leq \Delta\sigma_0^g \tag{19}$$

It is important to point out here that, as it is postulated by the TCD, under Mode I cyclic loading both $\Delta\sigma_0^g$ and ℓ must be determined by post-processing experimental results generated under the same load ratio as the one characterising the load history that is applied to the component being assessed.

Turning to the multiaxial fatigue case, consider now the notched component of Figure 4b which is assumed to be subjected to a complex system of time-variable forces and moments. By post-processing the results from a gradient elasticity FE model, the gradient-enriched linear-elastic stress state at the hot-spot can be expressed as follows (Fig. 4b):

$$\left[\sigma^g(t)\right] = \begin{bmatrix} \sigma_x^g(t) & \tau_{xy}^g(t) & \tau_{xz}^g(t) \\ \tau_{xy}^g(t) & \sigma_y^g(t) & \tau_{yz}^g(t) \\ \tau_{xz}^g(t) & \tau_{yz}^g(t) & \sigma_z^g(t) \end{bmatrix} \tag{20}$$

where t is time. In order to to use the MWCM to post-process gradient-enriched tensor (20) consistently, length scale parameter ℓ is recommended to be estimated via Eq. (18) by employing material fatigue properties determined under fully-reversed fatigue loading. This is due to the fact that, by nature, the MWCM is capable of directly modelling the mean stress effect in uniaxial/multiaxial fatigue [21]. Turning back to the design procedure summarised in Figure 4b, as soon as tensor (20) is known at any instant of the assessed load history, the

maximum shear stress amplitude, τ_a^g, and the relevant stress components perpendicular to the critical plane (i.e., $\sigma_{n,m}^g$ and $\sigma_{n,a}^g$) can directly be calculated according to one of the available methods [21, 19]. Gradient-enriched stress components τ_a^g, $\sigma_{n,m}^g$ and $\sigma_{n,a}^g$ allow then the effective value of the critical plane stress ratio, ρ_{eff}^g, to be calculated directly. Finally, the notched component being designed is assumed to be at its endurance limit as long as the following condition is assured:

$$\tau_{eq}^g = \tau_a^g - \left(\frac{\sigma_0^g}{2} - \tau_0^g \right) \cdot \rho_{eff}^g \leq \tau_0^g \text{ with } \rho_{eff}^g = \rho_{lim}^g \text{ for } \rho_{eff}^g > \rho_{lim}^g \tag{21}$$

where

$$\rho_{eff}^g = \frac{m \cdot \sigma_{n,m}^g + \sigma_{n,a}^g}{\tau_a^g} \; ; \; \rho_{lim}^g = \frac{\tau_0^g}{2\tau_0^g - \sigma_0^g} \tag{22}$$

As to the design procedure suggested to be followed to address the multiaxial fatigue problem (Fig. 4b), under complex time-variable load histories, the gradient-enriched stress state resulting from every applied force/moment can be computed separately. By so doing, the total gradient-enriched stress tensor at the hot-spot can then be calculated *a posteriori* by employing the superposition principle. This can be done because the proposed approach makes use of linear-elastic gradient-enriched stresses. Finally, this methodology based on the superposition principle has to be used by paying attention to keep unchanged the synchronism amongst the different forces and moments being assessed. This simple and standard procedure allows the presence of superimposed static stresses as well as the degree of non-proportionality of the applied load history to be taken into account accurately during the design process.

VALIDATION BY EXPERIMENTAL DATA

In order to check its accuracy and reliability, the proposed design approach (Fig. 4) was used to post-process a large number of experimental data taken from the literature. The considered results were generated by testing, under both uniaxial and multiaxial cyclic loading, metallic specimens containing different geometrical features. Table 1 and 2 summarise the experimental results which were used to perform the validation exercise that will be discussed in the following sub-sections. The reader is also referred to Refs [21, 23, 27, 33] for a detailed summary of the data sets listed in Tables 1 and 2.

Mode I Fatigue Loading

The accuracy of the proposed approach in estimating high-cycle fatigue strength of notched components was initially checked by considering a number of experimental results generated by testing flat and cylindrical notched specimens subjected to uniaxial cyclic loading. For the Mode I loading case, the error was calculated as follows:

$$E_\sigma[\%] = \frac{\Delta\sigma_y^g - \Delta\sigma_o^g}{\Delta\sigma_o^g} \cdot 100 \tag{23}$$

where $\Delta\sigma_y^g$ is the range of the gradient-enriched stress at the notch tip (see Figure 4a).

According to definition (23), a positive value of E_σ indicates a conservative estimate, whereas a negative value of this error index denotes a non-conservative prediction.

The specimens being analysed were subdivided into three groups, i.e. flat plates with central notch (CNP), flat plates with double edge notch (DENP) and cylindrical bars with circumferential notch (CNB). For any considered data sets, Table 1 lists the relevant material fatigue properties, the maximum and minimum length of the investigated root radius, r_n, the geometry of the tested notched specimens, and the type of applied loading.

Turning to the gradient elasticity FE analyses, since the considered notched flat specimens were symmetrical about two axes, only a quarter of the CNP and DENP samples was modelled. Similarly, in the case of the CNB specimens only half of the longitudinal section was modelled by using axisymmetric elements. Independently of the specific geometry, under-integrated bi-quadratic quadrilateral elements were used. The mesh in the vicinity of the stress concentrators was gradually refined according to the recommendations on optimal element size given in Refs [12, 13]. In particular, in the highly stressed regions the average mesh size was equal to about 0.025 mm, with the minimum size approaching 0.002 mm (Fig. 5). To apply the staggered formulation of Ru and Aifantis' theory, two sets of boundary conditions were employed as follows. For the first step, the usual homogeneous essential boundary conditions of classic elasticity were used to restore the symmetry of the problem. In the second step, homogeneous natural boundary conditions were applied throughout, so that $n_m \ell^2 \sigma_{ij,m}^g = 0$ (where n is the outward normal to the boundary). The gradient elasticity FE models used to determine the relevant stress states at the notch tips (Fig. 4a) were solved by using an in-house FE code developed by the authors.

The charts of Figure 5 show some examples of the linear-elastic stress fields obtained by using gradient elasticity according to the numerical procedure described in the previous paragraph. In particular, the diagrams of Figure 5a were determined by considering CNP specimens of SM41B [36, 37] with central hole having radius, r_n, equal to 0.16 mm (K_t=9.8) and 3 mm (K_t=3), respectively. The stress fields reported in Figure 5b were calculated instead by modelling the DENP samples of mild steel [38, 39] with notch root radius, r_n, equal to 0.1 mm (K_t=14.9) as well as to 1.27 mm (K_t=4.75). In both cases length scale parameter ℓ was directly estimate from $\Delta\sigma_o$ and ΔK_{th} via Eq. (18). These four diagrams clearly show gradient elasticity's smoothing effect, this resulting in stress fields having, in the vicinity of the notch tip, magnitude lover than the corresponding ones calculated according to continuum mechanics.

At the beginning of the last century, Neuber [1] formulated his well-known notch fatigue approach by taking as a starting point the idea that the stress in the vicinity of notches does not reach values as high as those which are estimated by using classic continuum mechanics. According to this intuition, he proposed to calculate a quantity representative of the real stress states in the vicinity of the crack initiation locations by averaging the stress fields close to the notch apices over materials units (that is, crystals or structural particles). In other words, Neuber suggested calculating an effective stress to be used to design notched components against high-cycle fatigue by considering finite volumes and not infinitesimal volumes as postulated by classic continuum mechanics. The charts of Figure 5 make it evident that gradient elasticity is a powerful numerical tool allowing Neuber's idea to be implemented efficiently, the size of the finite volumes used to determine the relevant stress fields being related to characteristic length ℓ.

The error diagram of Figure 6 summarises the overall accuracy which was obtained by using gradient elasticity according to the procedure described in Figure 4a. This diagram makes it evident that the estimates are characterised by an E_σ value falling mainly within an error interval ranging between −10% and +30%. It is worth remembering here that the use of the conventional TCD is seen to result in predictions falling within an error interval of ±20% [48, 49]. This error level is considered to be acceptable since, in general, it is not possible to distinguish between an error of ±20% and an error of 0% due to those problems which are usually encountered during testing as well as during the numerical analyses [48]. Hence, it is possible to state that, as the conventional TCD, the systematic usage of the proposed approach resulted in predictions falling within an error range of 40%, with the average value of the error itself being shifted by 10% toward the conservative side. In other words, gradient elasticity employed according to the procedure summarised in Figure 4a is seen to result in an overall accuracy characterised by the same absolute scattering as the one obtained by applying the classic TCD, the estimates being slightly more conservative.

As to the predictions summarised in Figure 6, it is worth pointing out here that these estimates were obtained by using $\Delta\sigma_0^g$ as reference un-notched fatigue limit. Obviously, under axial loading, the same level of accuracy would be reached by using $\Delta\sigma_0$ instead of $\Delta\sigma_0^g$, since in the absence of stress gradients $\Delta\sigma_0^g$ is invariably equal to $\Delta\sigma_0$ (see Figure 3b). Turning to the notched specimens tested under rotating bending, Table 1 shows that for 0.45C steel and 0.36C steel the difference between $\Delta\sigma_0^g$ and $\Delta\sigma_0$ approaches 1%. This implies that using $\Delta\sigma_0$ as reference plain fatigue limit to assess these notched samples would result in the same overall level of accuracy as the one that was obtained by employing the gradient-enriched fatigue limits, $\Delta\sigma_0^g$. This confirms that gradient elasticity can be safely used to predict high-cycle fatigue strength by also employing the conventional un-notched fatigue limit as reference material strength.

Multiaxial fatigue approach

After investigating the accuracy of the Mode I formalisation of the proposed approach, the subsequent step was checking whether gradient elasticity applied along with the MWCM (Fig. 4b) is successful also in estimating high-cycle fatigue strength under multiaxial fatigue loading. The experimental results summarised in Table 2 were generated by testing shafts with shoulder fillet (SSF) and circumferentially notched cylindrical bars (CNB) under in-phase and out-of-phase fully-reversed bending (or tension) and torsion. In order to check its accuracy in modelling the mean stress effect in fatigue, the proposed design approach was also employed to estimate the high-cycle fatigue strength of the notched samples of both S65A [47] and En3B [27] which were tested under biaxial cyclic loading with superimposed static stresses. For the re-analysed experimental results, Table 2 summarises the relevant material fatigue properties, the length of the assessed notch root radii, r_n, the geometry of the notched specimens, and the type of applied loading. As to the L values listed in this table, it is

worth observing that they were estimated [23, 27] by following a procedure based on the combined use of plain and notch fatigue limits [50].

Other than the results summarised in Table 2 and generated under multiaxial fatigue loading, the accuracy of gradient elasticity applied in conjunction with the MWCM was also checked against a number of experimental results generated by testing CNP and DENP specimens under uniaxial loading (refer to Table 1). The goal of this validation exercise was investigating whether this design approach is successful in taking into account the actual degree of multiaxiality of the gradient-enriched stress fields.

The gradient-enriched stress tensors at the hot-spots (Fig. 4b) were determined via 2D and 3D gradient elasticity FE models solved by using our in-house code. In the CNP and DENP samples, the gradient enriched stress distributions across the thickness were determined by solving three-dimensional FE models done considering one eighth of the specimens. These 3D solutions were obtained by discretising the domain with 10-noded (quadratic) tetrahedrons, a four-Gauss-point integration rule being employed to solve the two steps of the numerical problem – i.e., Eq. (3) and Eq. (5), respectively. In the 3D models, the average mesh size in the vicinity of the notch tips was equal to about 0.045 mm, with the minimum size approaching 0.008 mm (Fig. 7).

Turning to the notched cylindrical samples, only half of the longitudinal section of the investigated specimens was modelled by using under-integrated axisymmetric bi-quadratic quadrilateral elements, the mesh in the vicinity of the assessed stress concentrators being gradually refined until convergence occurred [13]. For these axisymmetric models the average mesh size in the highly stressed regions was equal to 0.015 mm, the minimum size being equal to about 0.001 mm (Fig. 8). As done for the Mode I loading specimens, also in this case the boundary conditions were taken as homogeneous essential to calculate the first step of the solution and homogeneous natural throughout to solve the second step of the numerical process. Finally, since the relevant stress states were calculated by solving

axisymmetric models, the total stress tensors at the hot-spots were determined for any considered multiaxial loading case by simply using the superposition principle.

As to the notched specimens with shoulder fillet (SSF), the hot-spot was positioned, within the fillet, in a material region close to the junction between the fillet itself and the net section of the samples. This is in agreement with the cracking behaviour observed by Gough [47]. In fact, nearly all the SSF samples he tested were seen to fail by a crack initiating at the junction of the fillet with the central portion of the specimens or slightly removed from that region and within the fillet.

The diagrams reported in Figure 7 show the through-thickness distribution of the gradient enriched stress components along the tip of the notch in the CNP specimens of SM41B [36, 37] loaded in cyclic tension-compression. The reported stress distributions (Figs 7b and 7d) confirm that in three-dimensional bodies the gradient enriched stress states at the tip of the notch (i.e., on the surface) are always multiaxial, even if the nominal loading being applied is uniaxial. This a consequence of the fact that, as schematically shown in Figure 3a, gradient elasticity acts as a numerical operator transferring the sub-surface stresses (which are, in the most general case, triaxial) onto the surface. In terms of fatigue assessment, this results in the fact that the hot-spots tend to move from the main surface toward the mid-section of the specimens (i.e., along axis z in Figure 7a). These is confirmed by the charts reported in Figures 7c and 7e: for the specimens with r_n=0.16 mm the hot spot - i.e., the material point experiencing the largest value of τ_{eq}^g calculated according to Eq. (21) - is at a distance from the main surface equal to 0.35 mm, whereas for the samples with r_n=3 mm it is positioned at the mid-section of the notched plate. A similar situation was also observed in the DENP specimens.

The charts reported in Figure 8 show the stress distributions along the notch bisector in CNB specimens loaded in bending, tension, and torsion. As to the stress analysis problem, it is interesting to observe here that, according to the way gradient elasticity manipulates the local stress fields, with ℓ>0 the gradient enriched stress state at the tip of a circumferential

notch in a cylindrical bar loaded either in bending, in tension, or in torsion is always multiaxial. In other words, in the investigated axisymmetric notched specimens, the gradient-enriched stress fields acting on the material in the vicinity of the hot-spots were always multiaxial, this holding true independently from the degree of multiaxiality characterising the nominal load history.

After determining the relevant gradient-enriched stress tensors at the hot-spots (Fig. 4b), the stress components relative to the critical plane (i.e., τ_a^g, $\sigma_{n,m}^g$ and $\sigma_{n,a}^g$) were calculated by using software Multi-FEAST (www.multi-feast.com). In particular, the amplitude of the gradient-enriched shear stress relative to the critical plane was determined according to the Maximum Variance Method [30, 31].

The error diagrams of Figure 9 summarise the overall accuracy which was obtained by using gradient elasticity in conjunction with the MWCM to post-process the considered data sets, with the error being defined as follows – see also Eq. (21):

$$E_\tau[\%] = \frac{\tau_{eq}^g - \tau_0^g}{\tau_0^g} \cdot 100 \tag{24}$$

According to definition (24), a positive value of this error index indicates a conservative estimate, whereas a negative value a non-conservative prediction.

As to the accuracy of the proposed approach (Fig. 4b), attention was initially focussed on those experimental results generated by testing CNP and DENP specimens under nominal uniaxial fatigue loading. As mentioned earlier, for these specimens the relevant gradient enriched stress fields were determined by solving 3D FE models. As shown in Figures 7c and 7e for two samples of SM41B [36, 37], the fatigue damage extent in CNP and DENP specimens loaded in cyclic tension-compression was estimated by considering that material point in the thickness experiencing the largest value of the equivalent shear stress amplitude, τ_{eq}^g, calculated according to Eq. (21). It is important to observe here that, to calculate τ_{eq}^g,

the gradient enriched plain torsional fatigue limits, τ_0^g, were estimated from the corresponding uniaxial ones according to von Mises' hypothesis. The error diagram reported in Figure 9a confirms that gradient elasticity applied along with the MWCM was successful in assessing the high-cycle fatigue strength of CNP and DENP specimens, the estimates falling within an error interval of ±20%.

Subsequently, attention was focussed on the experimental results generated by testing notched cylindrical specimens under uniaxial fatigue loading (i.e., either bending or tension-compression). The error chart of Figure 9b confirms that the use of the multiaxial formulation of the proposed approach resulted in highly accurate estimates also when it was employed to post-process the results from axisymmetric FE models. In particular, it is worth observing that accurate predictions were made not only under fully-reversed (R=1) uniaxial loading, but also in the presence of superimposed static stresses.

Turning to the torsional case, Figure 9b shows that the obtained estimates were, on average, characterised by a slightly higher degree of conservatism. This can be explained by observing that the TCD critical distance under torsion is seen to be larger than the corresponding value determined under uniaxial loading [51, 52]. Therefore, since in the proposed approach material characteristic length ℓ is directly derived from the TCD critical distance, L, determined under uniaxial fatigue loading, Eq. (18), the fact that under torsional loading the systematic usage of the proposed approach resulted in estimates characterised by a certain level of conservatism is not at all surprising.

As far as multiaxial load histories are concerned, the error chart of Figure 9b confirms that the use of the proposed approach resulted in estimates mainly falling within an error interval of ±20%, this holding true not only in the presence of out-of-phase loading, but also under non-zero mean stresses.

As to the prediction reported in the charts of Figure 9b, it is possible to observe that they were made by using σ_0^g and τ_0^g as reference fatigue strengths. Since, according to Table 2, the difference between conventional and gradient-enriched fatigue limits was always lower

than about 6% (with the average value approaching 1.5%), it is evident that using σ_o and τ_o instead would result in an overall accuracy similar to the one which was obtained by employing σ_o^g and τ_o^g. This further confirms that, in situations of practical interest, the proposed multiaxial fatigue design approach can safely be used by simply employing σ_o and τ_o as material reference strengths.

CONCLUSIONS

- Through the TCD's critical distance L, the gradient elasticity length scale parameter ℓ can directly be estimated from the plain fatigue limit and the threshold value of the stress intensity factor.

- Gradient elasticity allows high-cycle fatigue strength of notched components to be assessed accurately by directly post-processing the gradient enriched stress states determined, at the hot-spots, on the surface of the component being assessed.

- Under Mode I cyclic loading, the gradient-enriched hot spot stress perpendicular to the notch bisector can directly be used to estimate the extent of damage in the high-cycle fatigue regime.

- Gradient elasticity applied along with the MWCM is highly accurate in estimating high-cycle fatigue strength of notched components subjected to both uniaxial and multiaxial fatigue loading.

- Further research is required in this area to extend the use of the proposed methodology to the finite lifetime regime.

REFERENCES

[1] H. Neuber. Theory of notch stresses: principles for exact calculation of strength with reference to structural form and material. Springer Verlag, Berlin, 1958.

[2] R. E. Peterson. Notch-sensitivity. In G. Sines and J. L. Waisman, editors, Metal Fatigue, pages 293–306. McGraw Hill, New York, 1958.

[3] D. Taylor. The Theory of Critical Distances: A New Perspective in Fracture Mechanics. Elsevier, Oxford, UK, 2007.

[4] C. Q. Ru and E. C. Aifantis. A simple approach to solve boundary-value problems in gradient elasticity. Acta Mechanica, 101:59–68, 1993. doi: 10.1007/BF01175597.

[5] H. Askes, P. Livieri, L. Susmel, D. Taylor, and R. Tovo. Intrinsic material length, Theory of Critical Distances and Gradient Mechanics: analo¬gies and differences in processing linear-elastic crack tip stress fields. Fa¬tigue Fract. Engng. Mater. Struct., 36:39–55, 2012.

[6] L. Susmel, H. Askes, T. Bennett, and D. Taylor. Theory of Critical Distances versus Gradient Mechanics in modelling the transition from the short to long crack regime at the fatigue limit. Fatigue Fract. Engng. Mater. Struct., 36:861–869, 2013.

[7] Askes, H., Livieri, P., Susmel, L., Taylor, D., Tovo R. Intrinsic material length, Theory of Critical Distances and Gradient Mechanics: analogies and differences in processing linear-elastic crack tip stress fields. Fatigue Fract Engng Mater Struct. 36, pp. 39-55, 2013.

[8] Tovo R, Livieri P. An implicit gradient application to fatigue of sharp notches and weldments. Engng Frac Mech 2007;74 4:515-526.

[9] Livieri P, Tovo R. The effect of throat underflushing on the fatigue strength of fillet weldments. Fatigue Fract Engng Mater Struct 2013;36 9:884-892.

[10] E. C. Aifantis. On the role of gradients in the localization of deformation and fracture. Int. J. Eng. Sci., 30(10):1279–1299, 1992. doi: 10.1016/0020-7225(92)90141-3.

[11] S.B. Altan and E. C. Aifantis. On the structure of the mode III crack-tip in gradient elasticity. Scripta Metallurgica et Materialia, 26:319–324, 1992.

[12] C. Bagni and H. Askes. Unified finite element methodology for gradient elasticity. Computers and Structures, 160:100–110, 2015. doi: 10.1016/j.compstruc.2015.08.008.

[13] Bagni, C., Askes, H., Susmel L. Finite element technology for gradient elastic fracture mechanics. Procedia Materials Science 3, pp. 2042-2047, 2014.

[14] H. Askes, I. Morata, and E. C. Aifantis. Finite element analysis with staggered gradient elasticity. Comput. Struct., 86:1266–1279, 2008.

[15] H. Askes and E. C. Aifantis. Gradient elasticity in statics and dynamics: An overview of formulations, length scale identification procedures, finite element implementations and new results. Int. J. Solids Struct., 48(13): 1962–1990, 2011.

[16] H. Askes and I. Gitman. Non-singular stresses in gradient elasticity at bi-material interface with transverse crack. Int. J. Fract., 156:217–222, 2009.

[17] D. Taylor. Geometrical effects in fatigue: a unifying theoretical model. Int. J. Fatigue, 21:413–420, 1999. doi: 10.1016/S0142-1123(99)00007-9.

[18] El Haddad MH, Topper TH, Smith KN. Fatigue crack propagation of short cracks. J. Engng. Mater. Tech. (ASME Trans.) 1979;101:42-45.

[19] Tanaka K. Engineering formulae for fatigue strength reduction due to crack-like notches. Int J Fracture 1983;22:R39-R45.

[20] Sheppard SD. Field effects in fatigue crack initiation: long life fatigue strength. Trans. ASME. Journal of Mechanical Design 1991;113:188-194.

[21] Susmel, L., Multiaxial Notch Fatigue: from nominal to local stress-strain quantities. Woodhead & CRC, Cambridge, UK, ISBN: 1 84569 582 8, March 2009.

[22] Susmel, L., Taylor, D., Can the conventional High-Cycle Multiaxial Fatigue Criteria be re-interpreted in terms of the Theory of Critical Distances? Structural Durability & Health Monitoring, Vol. 2, No. 2, pp. 91-108, 2006.

[23] L. Susmel. A unifying approach to estimate the high-cycle fatigue strength of notched components subjected to both uniaxial and multiaxial cyclic loadings. Fatigue & Fracture of Engineering Materials & Structures, 27(5):391–411, 2004.

[24] Susmel, L., Taylor, D., Two methods for predicting the multiaxial fatigue limits of sharp notches. Fatigue Fract. Engng. Mater. Struct. 26, pp. 821-833, 2003.

[25] Susmel, L., Lazzarin, P., A Bi-Parametric Modified Wöhler Curve for High Cycle Multiaxial Fatigue Assessment. Fatigue Fract. Engng. Mater. Struct., Vol. 25, pp. 63-78, 2002.

[26] Susmel, L., Multiaxial Fatigue Limits and Material Sensitivity to Non-Zero Mean Stresses Normal to the Critical Planes. Fatigue Fract Engng Mater Struct 31, pp. 295-309, 2008.

[27] Susmel, L., Taylor, D. (2008) The Modified Wöhler Curve Method applied along with the Theory of Critical Distances to estimate finite life of notched components subjected to complex multiaxial loading paths. Fatigue & Fracture of Engineering Materials & Structures 31 12, pp. 1047-1064.

[28] Susmel, L., Tovo, R., Lazzarin, P. (2005) The mean stress effect on the high-cycle fatigue strength from a multiaxial fatigue point of view. International Journal of Fatigue 27, pp. 928-943.

[29] Kaufman, R. P., Topper T. (2003) The influence of static mean stresses applied normal to the maximum shear planes in multiaxial fatigue. In: Biaxial and Multiaxial fatigue and Fracture, Edited by A. Carpinteri, M. de Freitas and A. Spagnoli, Elsevier and ESIS, pp. 123-143.

[30] Susmel L., A simple and efficient numerical algorithm to determine the orientation of the critical plane in multiaxial fatigue problems. International Journal of Fatigue 32, pp. 1875–1883, 2010.

[31] Susmel, L., Tovo, R., Socie, D. F. Estimating the orientation of Stage I crack paths through the direction of maximum variance of the resolved shear stress. Int J Fatigue 58, pp. 94–101, 2014.

[32] Jadallah, O., Bagni, C., Askes, H., Susmel, L. Microstructural length scale parameters to model the high-cycle fatigue behaviour of notched plain concrete. International Journal of Fatigue, 82, pp. 708-720, 2016.

[33] B. Aztori, P. Lazzarin, and G. Meneghetti. Fracture mechanics and notch sensitivity. Fatigue Fract. Engng. Mater. Struct., 26:257–267, 2003.

[34] DuQuesnay D. L., Yu M., Topper T.H. (1988) An analysis of notch size effect on the fatigue limit. J. Testing Eval. 4, 375-385.

[35] El Haddad M. H. (1978) A study of the growth of short fatigue cracks based on fracture mechanics. Ph. D. Thesis, University of Waterloo, Waterloo, Ontario, 1978.

[36] Tanaka K., Nakai Y. (1983) Propagation and non-propagation of short fatigue cracks at a sharp notch. Fatigue Fract. Engng. Mater. Struct. 6, 315-327.

[37] Tanaka K., Akiniwa Y. (1987) Notch geometry effect on propagation threshold of short fatigue cracks in notched components. In: Fatigue '87, Vol. II, Edited by R. O. Ritchie and E. A. Starke Jr., 3th Int. Conf. on Fatigue and Fracture Thresholds, 739-748.

[38] Frost N. E. (1957) A relation between the critical alternating propagation stress and crack length for mild steel. In: Proc. Inst. Mech. Engrs., 173, 811-834.

[39] Harkegard G. (1981) An effective stress intensity factor and the determination of the notched fatigue limit. In: Fatigue Thresholds: Fundamentals and Engineering Applications, Vol. II (Ed. by J. Backlund, A. F. Blom and C. J. Beevers), Chameleon Press Ltd, London, 867-879.

[40] Frost N. E. (1957) Non-Propagating Cracks in Vee-Notched Specimens Subjected to Fatigue loadings. The Aeronautical Quarterly VIII, 1-20.

[41] Lukas, P., Kunz, L., Weiss, B., Stickler, R. (1986) Non-damaging notches in fatigue. Fatigue Fract. Engng Mater. Struct. 9, 195-204.

[42] Ting, J. C. and Lawrence, F. V. (1993) A crack closure model for predicting the threshold stresses of notches. Fatigue Fract. Engng Mater. Struct. 16, 93-114.

[43] Harkegard, G. (1981) An effective stress intensity factor andthe determination of the notched fatigue limit. In: Fatigue Thresholds: Fundamentals and Engineering Applications, Vol.II (Edited by J. Backlund, A. F. Blom and C. J. Beevers) Chameleon Press Ltd, London. pp. 867-879.

[44] Nisitani, H. and Endo, M. (1988) Unified treatment of deep and shallow notches in rotating bending fatigue. In: Basic Questions in Fatigue, Vol. I, ASTM STP 924, pp. 136-153.

[45] Kurath P., Downing S. D., Galliart D. R. (1989) Summary of Non-Hardened Notched Shaft Round Robin Program. In: Multiaxial Fatigue, Edited by G. E. Leese and D. F. Socie. Society of Automotive Engineers, AE-14, 13-32.

[46] Sonsino C. M. (1994) Fatigue Behaviour of Welded Components Under Complex Elasto-Plastic Multiaxial Deformation, LBF-Bericht, Nr. 6078.

[47] Gough H. J. (1949) Engineering Steels under Combined Cyclic and Static Stresses. In: Proc. Inst. Mech. Engrs. 160, 417-440.

[48] Taylor, D., Wang, G. (2000) The validation of some methods of notch fatigue analysis. Fatigue & Fracture of Engineering Materials & Structures 23, pp. 387–394.

[49] Susmel, L., Taylor, D. (2003) Fatigue Design in the Presence of Stress Concentrations. International Journal of Strain Analysis for Engineering Components 38 5, pp. 443-452.

[50] L. Susmel and D. Taylor. The Theory of Critical Distances as an alternative experimental strategy for the determination of KIC and ΔKth. Engineering Fracture Mechanics, 77:1492–1501, 2010. doi: 10.1016/j.engfracmech.2010.04.016.

[51] L. Susmel, D. Taylor. A simplified approach to apply the theory of critical distances to notched components under torsional fatigue loading. Int J Fatigue, 28 (2006), pp. 417–430.

[52] L. Susmel, D. Taylor. The Theory of Critical Distances to estimate finite lifetime of notched components subjected to constant and variable amplitude torsional loading. Engineering Fracture Mechanics. Volume 98, January 2013, Pages 64–79.

List of Captions

Tables

Material	Ref.	R	$\Delta\sigma_o$ [MPa]	$\Delta\sigma_o^g$ [MPa]	ΔK_{th} [MPa]	L [mm]	ℓ [mm]	Specimen Type[a]	Load Type[b]	r_n [mm]
SAE 1045	[34]	-1	608	608	13.6	0.159	0.056	CNP	Ax	0.12-2.5
Al 2024-T351	[34]	-1	248	248	5.0	0.129	0.046	CNP	Ax	0.12-1.5
G40.11	[35]	-1	464	464	15.9	0.374	0.132	CNP	Ax	0.2-4.8
SM41B	[36, 37]	-1	326	326	12.4	0.458	0.162	CNP	Ax	0.16-3.0
Mild Steel	[38, 39]	-1	420	420	12.8	0.296	0.105	DENP/CNB	Ax	0.05-7.62
NiCr Steel	[40]	-1	1000	1000	12.8	0.085	0.030	CNB	Ax	0.05-0.13
Steel 15313	[41]	-1	440	440	12.0	0.237	0.084	CNB	Ax	0.03-0.76
AISI 304	[42, 43]	-1	720	720	12.0	0.110	0.039	CNB	Ax	0.04
0.45 C Steel	[44]	-1	582	575.5	8.1	0.061	0.022	CNB	RB	0.01-0.6
0.36 C Steel	[44]	-1	446	442	7.6	0.092	0.033	CNB	RB	0.2

[a]CNP=Center Notch in flat Plate; DENP=Double Edge Notch in flat Plate; CNB=Circumferential Notch in cylindrical Bar
[b]Ax=Axial loading; RB=Rotating Bending

**Table 1.** Summary of the experimental results generated under uniaxial fatigue loading.

Material	Ref.	R	σ_0 [MPa]	σ_0^g [MPa]	τ_0 [MPa]	τ_0^g [MPa]	m	L [mm]	ℓ [mm]	Specimen Type[a]	Load Type[b]	r_n [mm]
SAE 1045	[45]	-1	304	303.1	176	175.5	-	0.159	0.056	SSF	B-T	5
Ck 45	[46]	-1	304	303.1	176	175.5	-	0.159	0.056	SSF	B-T	5
S65A	[47]	-1	584	581.6	371	369.7	0.37	0.056	0.020	SSF	B-T	0.838
0.4% C Steel	[47]	-1	332	325.1	207	203.1	-	0.178	0.063	CNB	B-T	0.005
3% Ni Steel	[47]	-1	343	337.2	205	201.9	-	0.144	0.051	CNB	B-T	0.005
3/3.5% Ni Steel	[47]	-1	352	330.6	267	252.6	-	0.516	0.182	CNB	B-T	0.01
Cr-Va Steel	[48]	-1	429	423.9	258	255.2	-	0.101	0.036	CNB	B-T	0.011
3.5% NiCr Steel (normal impact)	[48]	-1	540	530.5	352	346.4	-	0.150	0.053	CNB	B-T	0.022
3.5% NiCr Steel (low impact)	[48]	-1	509	502.5	324	320.2	-	0.109	0.039	CNB	B-T	0.022
NiCrMo Steel (75-80 tons)	[48]	-1	594	586.6	343	339.1	-	0.106	0.037	CNB	B-T	0.031
En3B	[27]	-1, 0	346	346	268	266.5	0.22	0.048	0.017	CNB	Ax-T	0.2, 1.25, 4.0

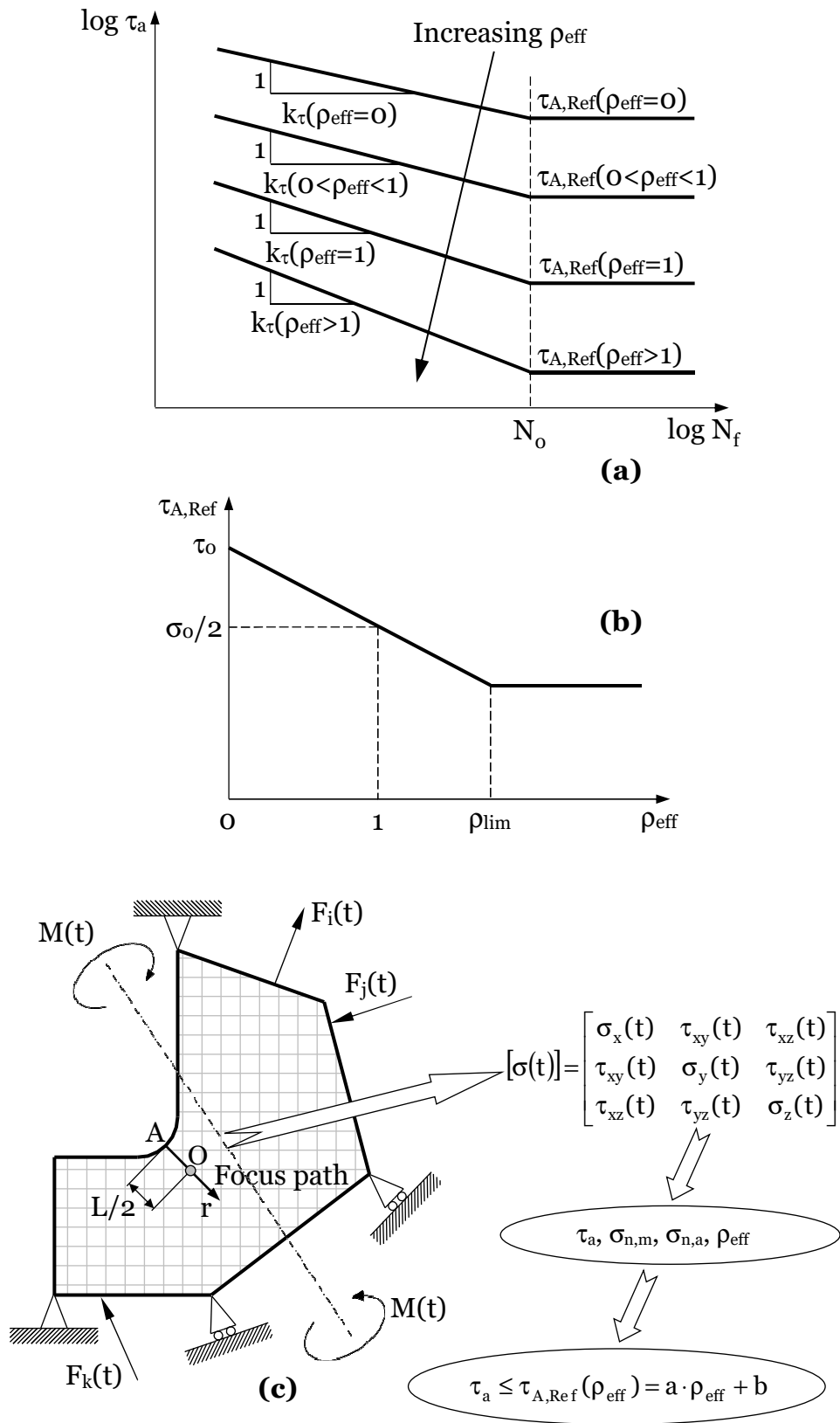[a]SSF=cylindrical Shaft with Shoulder Fillet; CNB=Circumferential Notch in cylindrical Bar
[b]Ax=Axial loading; B=Bending; T=Torsion

Table 2. Summary of the experimental results generated under multiaxial fatigue loading.
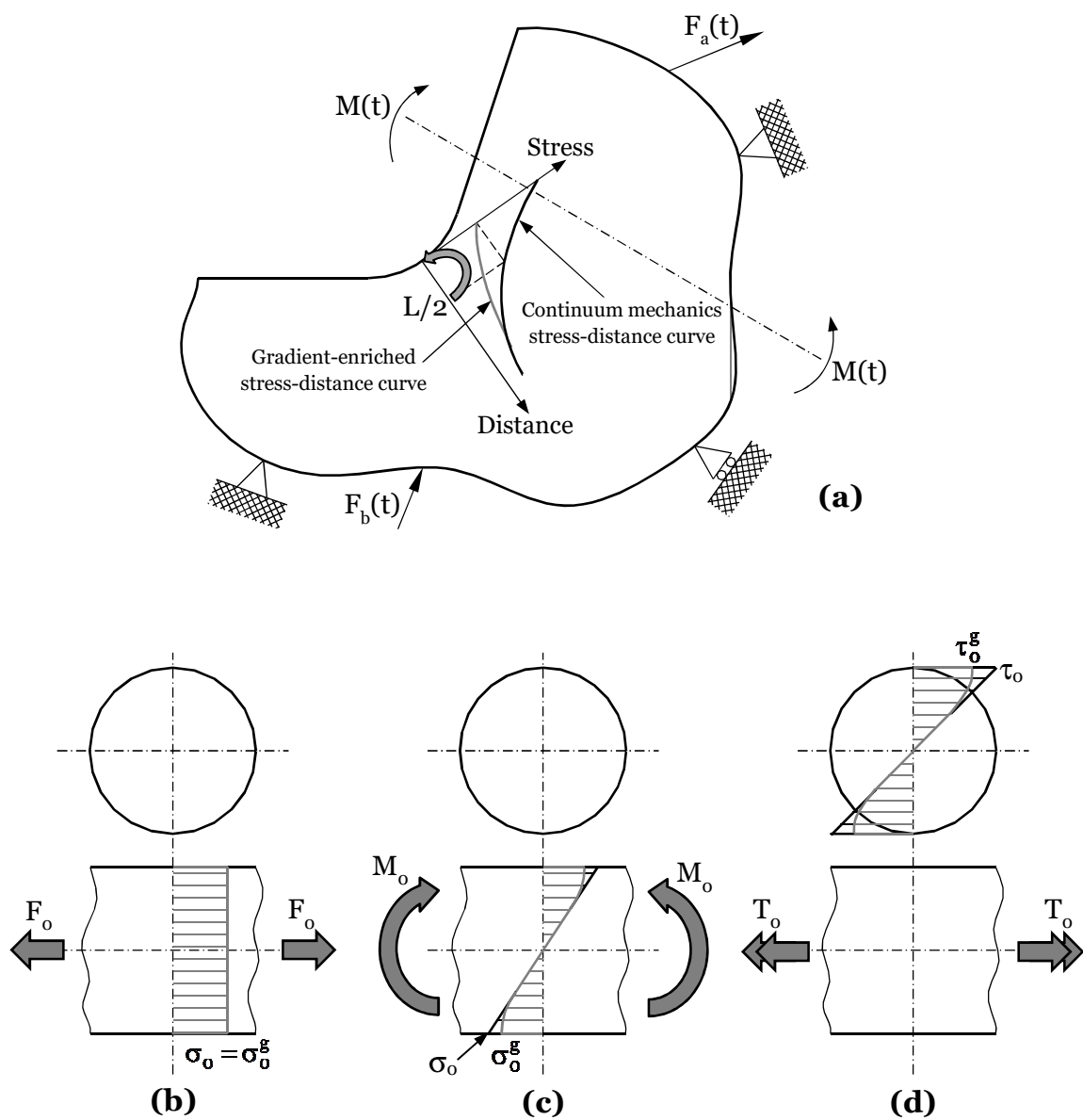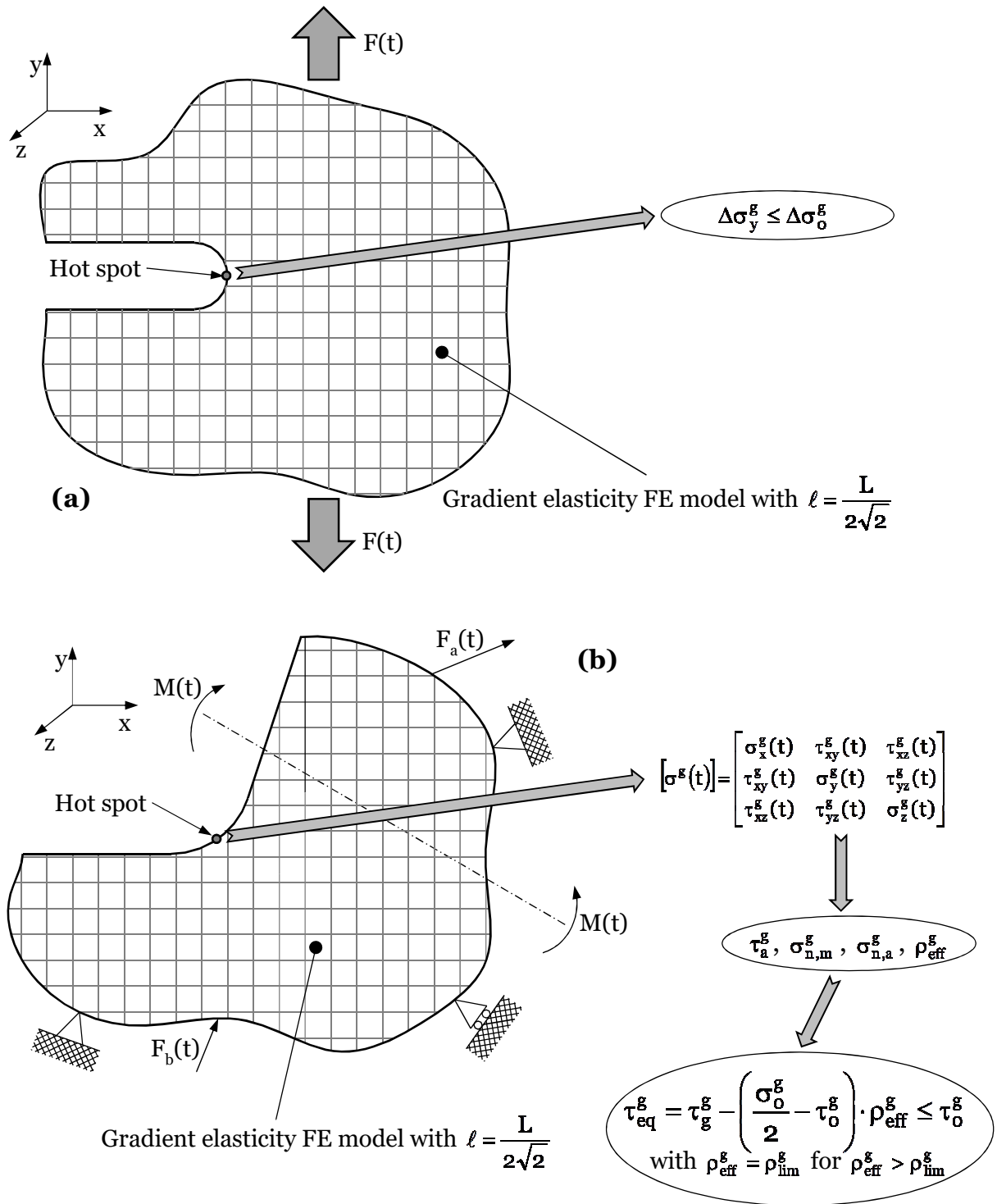
Figures
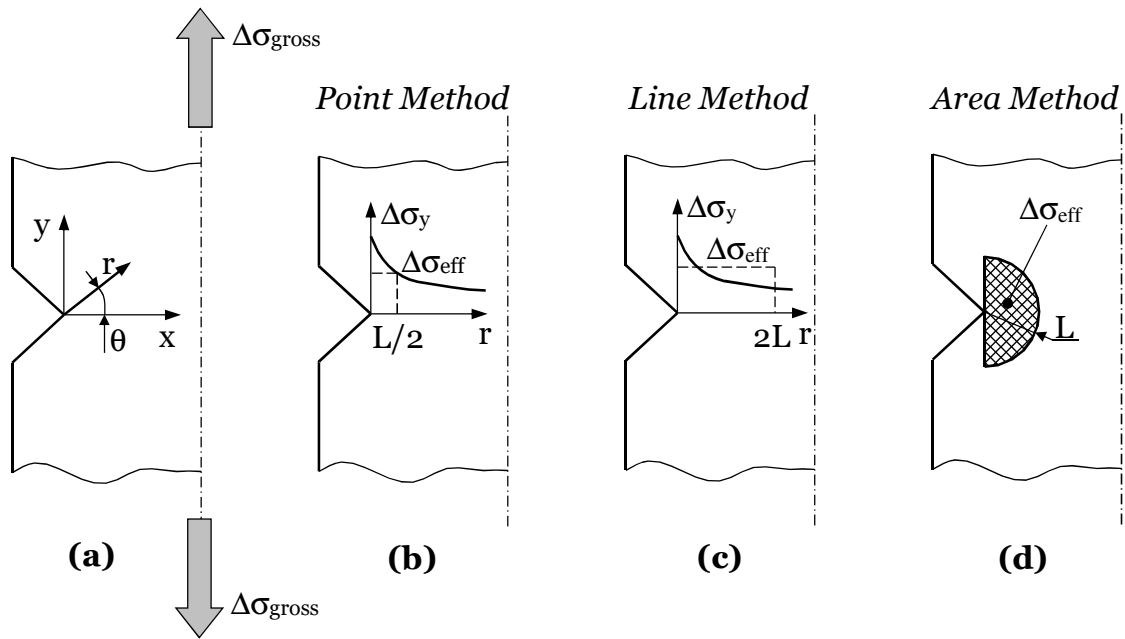
Figure 1. Different formalisations of the Theory of Critical Distances under Mode I fatigue loading.

Figure 2: Modified Wöhler curves (a), the $\tau_{A,Ref}$ vs. ρ_{eff} diagram (b) and in-field use of the MWCM applied along with the PM to estimate notch fatigue limits (c).

Figure 3. Gradient-enriched notch tip stress vs. PM effective stress (a); conventional and gradient-enriched un-notched fatigue (endurance) limits under cyclic axial loading (b), cyclic bending (c) and cyclic torsion (d).

Figure 4. In-field use of gradient elasticity to estimate notch fatigue (endurance) limits.
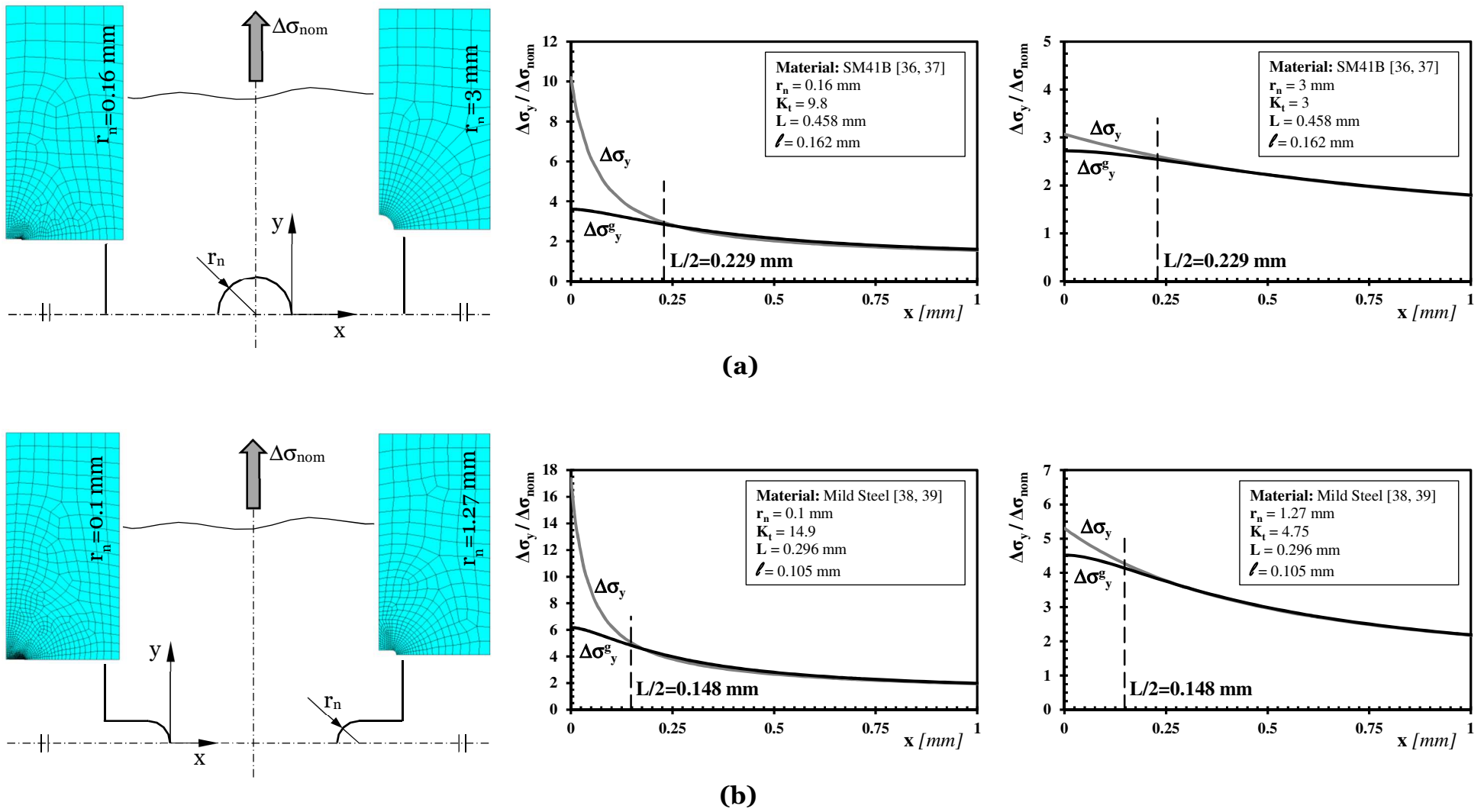
Figure 5: Stress distributions along the notch bisector in CNP (a) and DENP (b) specimens subjected to cyclic axial loading.
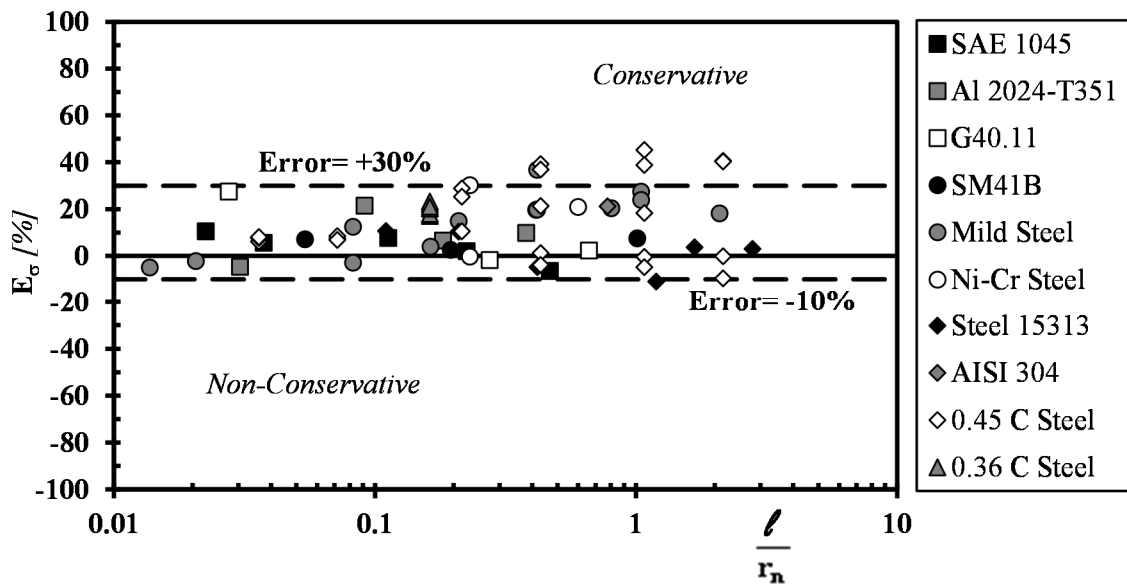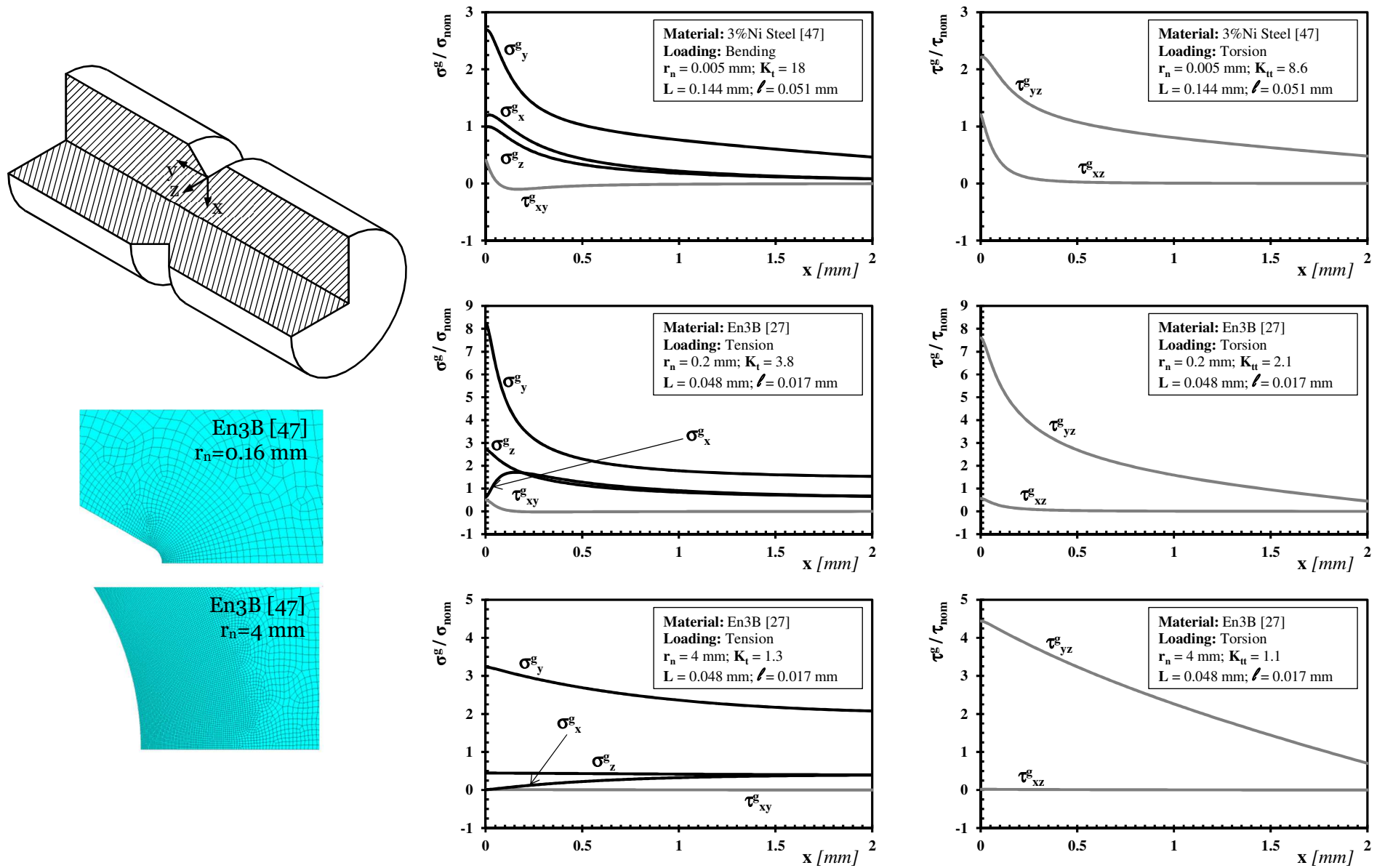
Figure 6. Accuracy of the proposed design method (Fig. 4a) in estimating high-cycle fatigue strength of notched specimens subjected to fully-reversed Mode I cyclic loading.
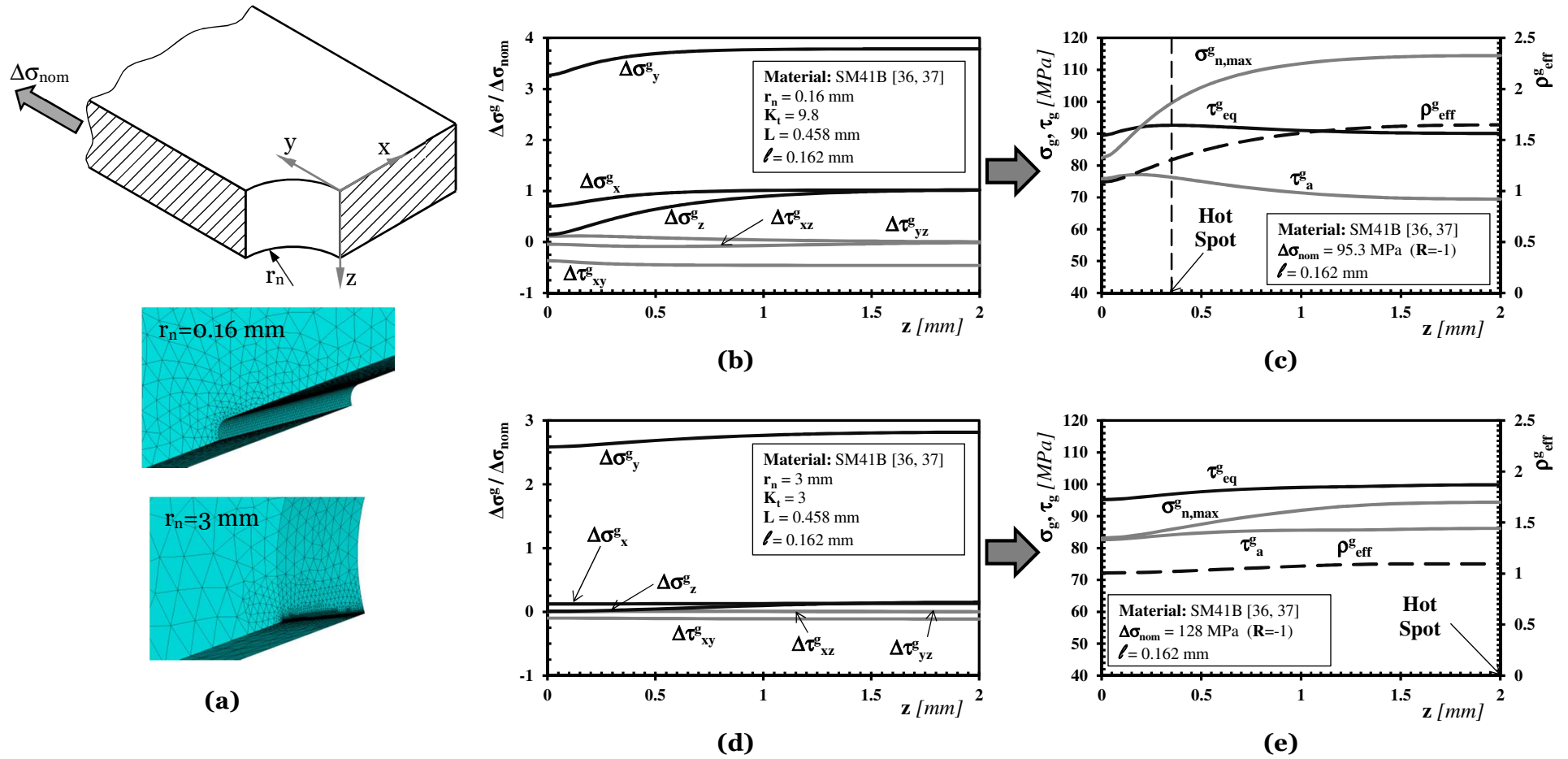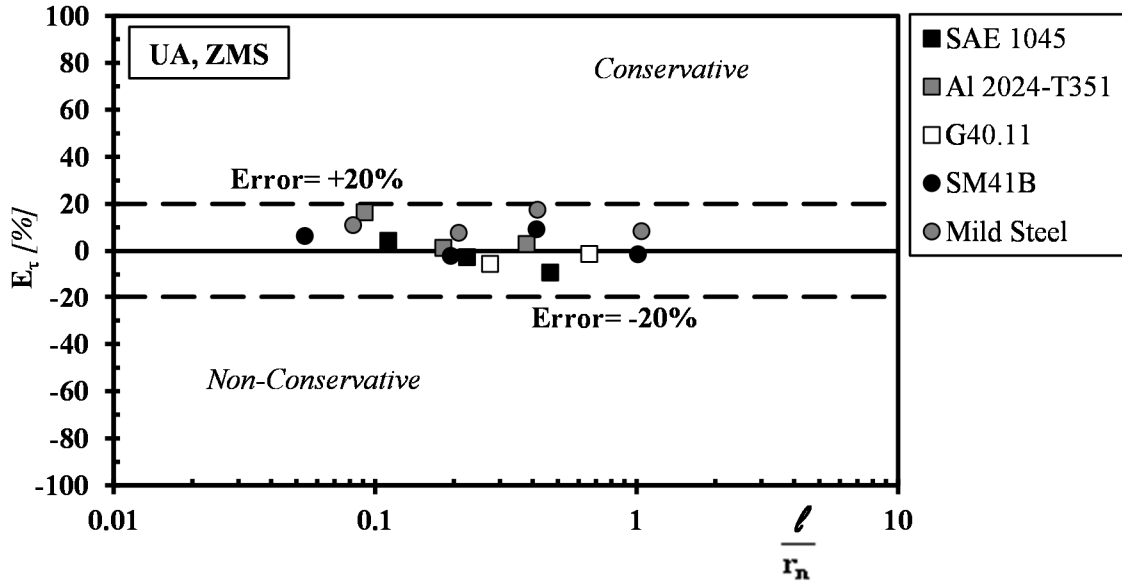
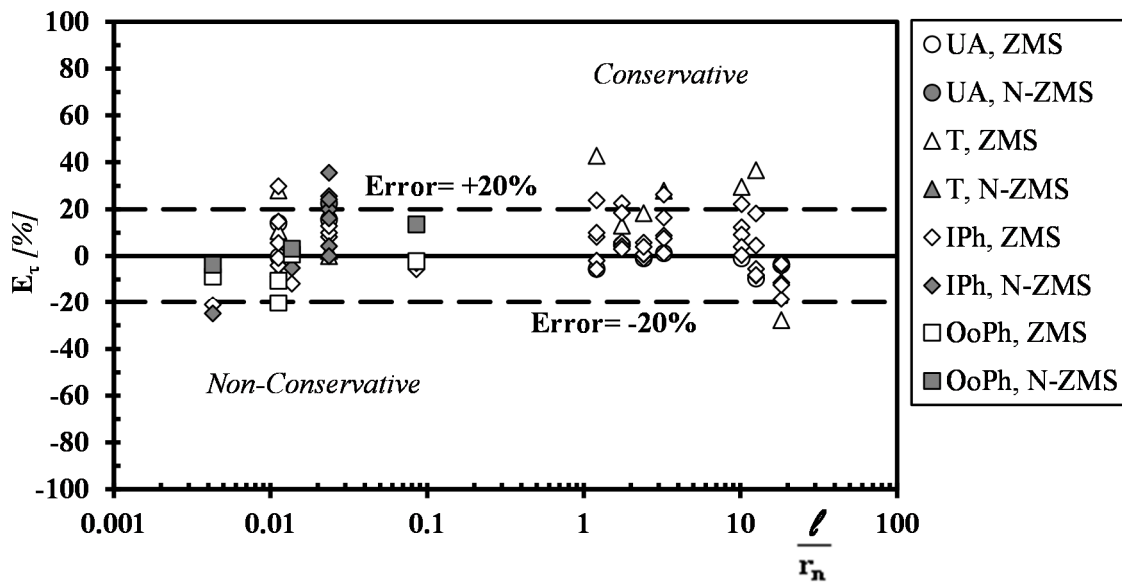**Figure 7:** Stress distributions along the notch edge in CNP specimens subjected to cyclic axial loading.

Figure 8: Stress distributions along the notch bisector in CNB specimens loaded in bending, tension, and torsion.

Figure 9. Accuracy of gradient elasticity applied along with the MWCM (Fig. 4b) in estimating high-cycle fatigue strength of notched specimens subjected to uniaxial/multiaxial fatigue loading (UA=uniaxial loading; T=torsional loading; IPh=In-Phase loading; OoPh=Out-of-Phase loading; ZMS=Zero Mean Stress; N-ZMS=Non-Zero Mean Stress).